

Pulsational instability domain of δ Scuti variables

A. A. Pamyatnykh

*N. Copernicus Astronomical Center, Polish Academy of Sciences,
Bartycka 18, 00-716 Warszawa, Poland*

*Institute of Astronomy, Russian Academy of Sciences,
Pyatnitskaya 48, 109017 Moscow, Russia*

*Institute of Astronomy, University of Vienna,
Türkenschanzstr. 17, A-1180 Wien, Austria*

Abstract.

An updated theoretical instability domain of the δ Scuti star models in the Hertzsprung-Russell diagram, in the $\log g - \log T_{\text{eff}}$ diagram and in diagrams for dereddened $wby\beta$ photometric indices is presented. The sensitivity of both the position of the evolutionary tracks and the Blue Edge of the instability domain to changes in the chemical composition parameters (X, Z) and to changes in the convection theory parameters (mixing-length in the stellar envelope, the extent of the overshooting from the convective core) is discussed.

1. Introduction

This paper continues the study of the pulsational instability domains in the upper main sequence (Pamyatnykh 1999, Paper I hereafter). In Paper I we considered updated theoretical instability domains in the Hertzsprung-Russell and in the $\log g - \log T_{\text{eff}}$ diagrams for models of β Cephei and SPB stars and studied the influence of variations of global input parameters (initial chemical composition, opacity data, efficiency of the overshooting from stellar convective cores) on the evolutionary models and their oscillations. Here we present the results of a similar study for models of δ Scuti stars. Our main goal is to demonstrate the influence of the choice of global parameters on the position of the hotter border (Blue Edge) of the δ Scuti instability domain. Linear nonadiabatic oscillation analyses using the simplest assumption about the interaction between convection and pulsation (namely, an assumption about frozen-in convective energy flux during an oscillation cycle) do not allow us to determine the position of the cooler instability edge (Red Edge). Therefore, in all diagrams we use an empirical Red Edge following Rodriguez et al. (1994) and Breger (1979) (note that M. Breger in his review in these Proceedings gives a similar but slightly steeper Red Edge). Recent successful theoretical predictions of the return to stability at the cool boundary of the instability strip are presented by G. Houdek in these Proceedings. Perturbations of the turbulent pressure of convection were found to be the main contributor to the damping of the pulsations.

There have been other general studies of the δ Scuti instability domain. We note the very important work by Stellingwerf (1979), who explained the different morphology of the blue edges calculated for different overtones of radial pulsations. We confirm his results qualitatively in Section 3. Li & Stix (1994) and Marconi & Palla (1998) used the OPAL opacity data in their computations of the position of the instability domain. In a paper about slowly pulsating B-type stars, Dziembowski, Moskalik & Pamyatnykh (1993) presented an HR diagram where the Blue Edge of the δ Scuti instability domain was also shown (Fig. 6 of the cited paper). Their results were obtained with an earlier version of the OPAL opacities. We also mention our old results on the blue edges of the instability domain computed with the Los Alamos opacities (Pamyatnykh 1975). The first general reviews on δ Scuti variables, in which theoretical aspects of the pulsations were outlined, were published by Baglin et al. (1973) and Breger (1979).

1.1. Models and their oscillations

The models of 1.3–3.0 M_{\odot} stars on the main sequence (MS) and in post-MS evolutionary stages were constructed using a standard stellar evolution code which was developed in its original version by B. Paczyński, R. Sienkiewicz and M. Kozłowski (private communication). The same code was used in Paper I and in our recent seismological studies on individual variables and on period changes in δ Scuti stars (see Breger et al. 1999 and references therein). We used the most recent versions of the OPAL and OP opacities (Iglesias & Rogers 1996 and Seaton 1996, respectively), supplemented with the low-temperature data of Alexander & Ferguson (1994). In all computations the OPAL equation of state was used (Rogers et al. 1996). The nuclear reaction rates are the same as used by Bahcall and Pinsonneault (1995).

In one series of the computations the effects of uniform (solid-body) stellar rotation were taken into account, assuming that the star conserves its global angular momentum during evolution from the Zero-Age Main Sequence.

In another series of the computations the possibility of overshooting from the convective core was taken into account.

The input parameters for evolutionary model sequences are total mass, M , initial values for hydrogen abundance, X , and the heavy element abundance, Z . The initial heavy element mixture is that of Grevesse & Noels (1993). The computations were performed starting from chemically uniform models on the Zero-Age Main Sequence (ZAMS). In the stellar envelope, the standard mixing-length theory of convection with the mixing-length parameter $\alpha = 1.0$ was used.

To test the effect of the mixing-length parameter choice on the model structure and stability, we computed one family of the models assuming pure radiative energy transfer in the stellar envelope (i.e., $\alpha = 0$).

As in Paper I, we studied only low-degree oscillations ($\ell \leq 2$), which are those most suitable for photometric detection; the excitation and visibility of high degree modes in δ Scuti and other variables is considered in detail by Balona & Dziembowski (1999). A linear nonadiabatic analysis of the oscillations was performed using a code developed by W. Dziembowski (for a general description see Dziembowski 1977). The effects of slow rotation on the oscillation frequencies

were treated up to third order in the rotational velocity (Dziembowski & Goode 1992, Soufi et al. 1998)¹.

In the next section an analogy between δ Scuti and β Cephei oscillations is demonstrated. Sect. 3 contains our main results on the δ Scuti instability domain assuming a standard evolutionary treatment of nonrotating stellar models without overshooting. The comparison with observational data is also given in this section using various diagrams. In Sect. 4 we discuss the effects of stellar rotation, convective overshooting and the mixing-length parameter choice, and in Sect. 5 we examine the effect of variations in the chemical composition. Last section contains summary and also the discussion of the effect of using another set of stellar opacities, namely, OP opacities (Seaton 1996). Moreover, the problems of the study of the post-MS δ Scuti stars are outlined using data on the variable 4 Canum Venaticorum as an example. Much more detailed results of asteroseismological studies of individual δ Scuti stars are presented in the paper by J. A. Guzik et al. in these Proceedings.

2. An analogy between the δ Scuti and β Cephei variables

In the HR diagram, the δ Scuti stars are located in the lower part of the classical instability strip where stellar pulsations are excited by the well-known κ -mechanism acting in zones of partial ionization of hydrogen and helium (Baker & Kippenhahn 1962, 1965; see also Cox 1963, Zhevakin 1963 and references therein). Chevalier (1971) was the first who explicitly studied pulsations of a δ Scuti star model and concluded that they are excited by the κ -mechanism acting in the second helium ionization zone.

The oscillations of the δ Scuti stars are similar in many aspects to those of the β Cephei variables because in both cases low-order acoustic and gravity modes are excited by the same classical κ -mechanism. The main difference is that the oscillations of the β Cephei variables rely on a different opacity bump than those of the stars in the classical instability strip, where the δ Scuti variables are located. Also, the periods of both groups are similar (lines of constant period are approximately parallel to the main sequence, see Fig. 5 below). We note in this respect (see a review by M. Breger in these Proceedings), that the prototype of the δ Scuti group, δ Scuti itself, was placed initially among the β Canis Majoris (β Cephei) variables according to its period.

Some properties of the pulsations within the β Cephei and δ Scuti instability domains are demonstrated in Fig. 1, where the frequency oscillation spectra for stellar models of $12 M_{\odot}$ and $1.8 M_{\odot}$ during their evolution from the ZAMS to the TAMS are plotted. For radial modes ($\ell = 0$) we see an almost equidistant frequency separation between consecutive modes. The complicated patterns of nonradial modes are caused by evolutionary changes in the stellar interiors, in the region surrounding the convective core. Due to these changes, the p - and g -modes are not separated in frequency already in mid- or early-MS evolution,

¹As it is stressed by M.-J. Goupil et al. in these Proceedings, rotation is assumed slow enough so that it may be treated as a perturbation but fast enough so that higher effects beyond linear in the rotation rate are considered.

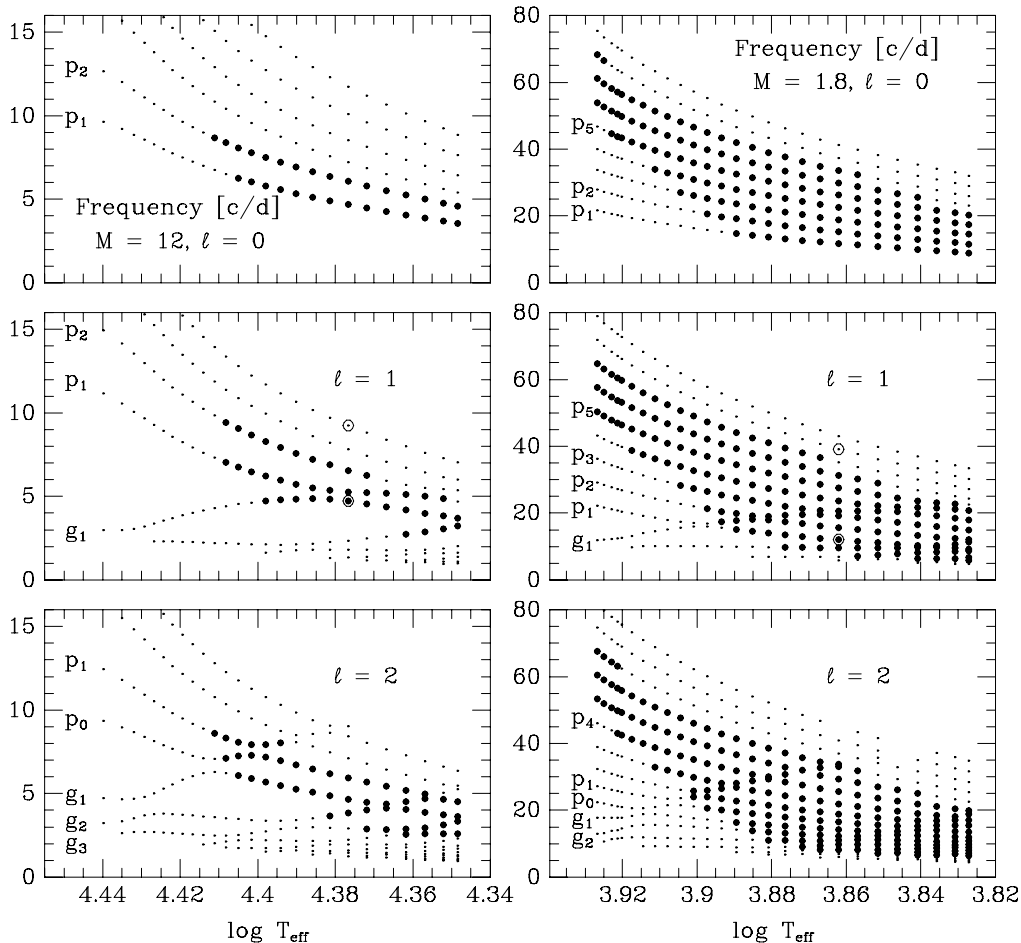


Figure 1. Frequencies of low-order p - and g -modes with low degree, ℓ , for models of 12 and $1.8 M_{\odot}$ in the Main Sequence evolutionary phase. In each panel, the leftmost and rightmost points correspond to the ZAMS and TAMS models, respectively. The large dots mark unstable modes. The large open circles in the $\ell = 1$ panels mark modes which are shown in Fig. 2.

and the phenomenon of “avoided crossing” between p - and g - modes takes place (Aizenman et al. 1977). This results in a mixed character of the low-order nonradial modes: they are similar to pure acoustic modes in the outer stellar layers and to pure gravity modes in the interiors. The high sensitivity of the avoided crossing occurrence to the extent of the convective core can be used to test the efficiency of overshooting from stellar convective cores, as was proposed by Dziembowski & Pamyatnykh (1991).

Both in the β Cephei and δ Scuti star models we find unstable low-order, low-degree p -, g - and mixed modes. There is at least one piece of observational evidence for the presence of g - or mixed modes in the frequency spectrum of the δ Scuti-type star FG Virginis (Breger et al. 1999).

We can see that the occurrence of instability during evolution away from the ZAMS does not depend essentially on mode degree, ℓ . Rather, it is determined primarily by the mode frequency. Therefore, when discussing the position of the δ Scuti instability domain, we restrict ourselves to the study of radial oscillations only.

We find that instability first appears in the acoustic overtones and then extends to gravity and/or mixed modes. As can also be seen from Fig. 1, the frequency range of the unstable modes in the $1.8 M_{\odot}$ models is more extended than that in the $12 M_{\odot}$ models. This is in agreement with the fact that the observed frequency range of the unstable modes is wider in δ Scuti than in β Cephei stars. An outstanding example is again FG Virginis, where 23 definitely detected modes span a frequency range of 9–34 c/d. 6 or 7 radial overtones are located in this frequency range (see Breger et al. 1999).

For an oscillation mode to be excited by the κ -mechanism, two conditions must be fulfilled in addition to the presence of a local opacity maximum: (i) the amplitude of oscillation must be relatively large and slowly varying in the potentially driving region, (ii) the thermal timescale in the driving zone, $\tau_{\text{th}}(r) = \int_r^R T c_p dM / L$, must be comparable or longer than the oscillation period.

If (ii) is not satisfied, the potentially driving region remains in thermal equilibrium during the pulsation cycle (neutral stability). This means that in order to excite the oscillations, the opacity bump has to be located at an optimal geometrical depth in the stellar envelope.

The efficiency of the κ -mechanism in representative models of β Cephei and δ Scuti variables is demonstrated in Fig. 2 (this figure is a subsection of Fig. 2 from Pamyatnykh 1999). The stars are located in the middle of the corresponding instability domains in the HR diagram. Both models have an initial chemical composition of $X = 0.70$ and $Z = 0.02$. The masses of the models are 12 and $1.8 M_{\odot}$, and the effective temperatures are 23800 K and 7280 K, respectively. All quantities are plotted as functions of temperature inside the models. Note that the value of the Rosseland mean opacity, κ , is systematically larger for smaller stellar mass, which reflects larger densities in the envelopes of these stars.

It is easy to see that the main driving in both models takes place in the layers with a steep radial gradient of the opacity derivative near the relevant opacity bump: it is the metal or Z bump for the β Cephei model and the bump due to the second helium ionization for the δ Scuti model.

The acoustic mode p_1 (as well as other low-order radial and nonradial modes) is unstable both in the β Cephei model and in the δ Scuti model. The following dipole ($\ell = 1$) modes are unstable in these representative models: low-order acoustic modes $p_1 - p_3$ with periods of 0.211 to 0.153 days in the β Cephei model, low-order modes $g_2, g_1, p_1 - p_6$ with periods of 0.104 to 0.052 days in the δ Scuti model.

The helium bump region, where pulsations of δ Scuti stars are driven, does not contribute to the work integral in the β Cephei model due to the very short thermal timescale there. However, the timescale requirement can be satisfied in B stars at the position of the metal bump.

In the model of a β Cephei star of $12M_{\odot}$, the thermal timescale there is comparable with periods of the low order p -modes. The higher-order acoustic

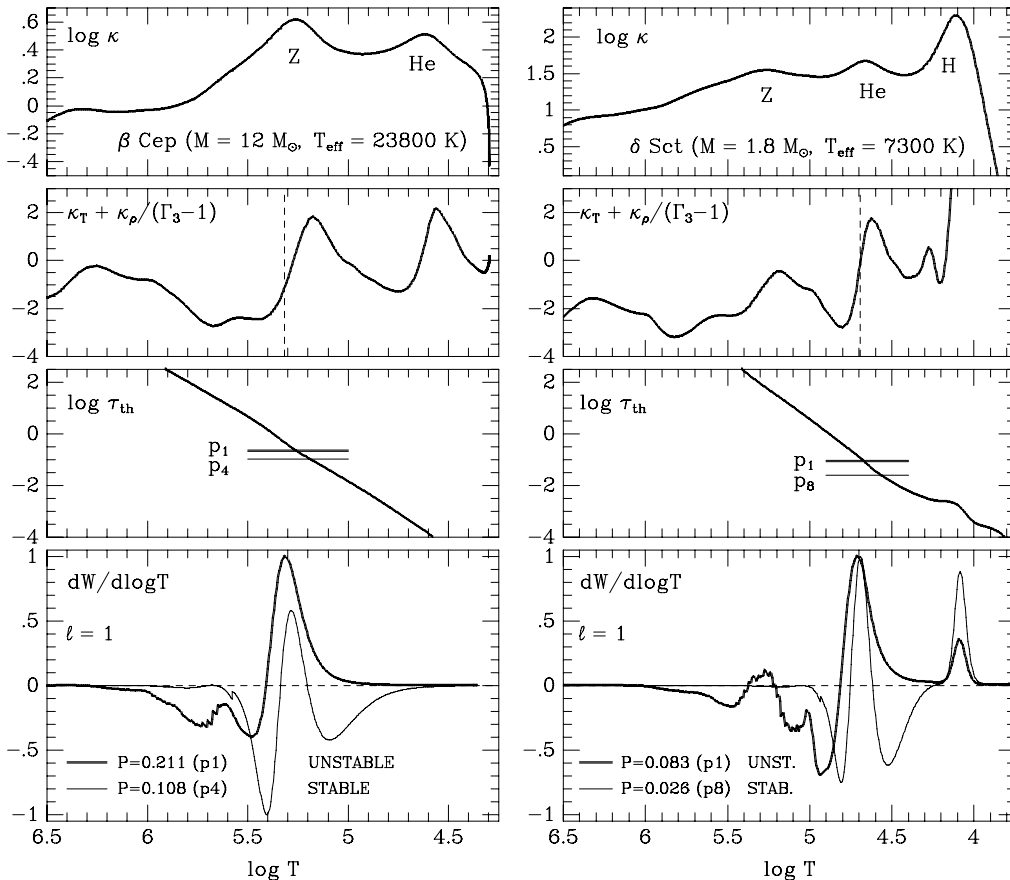


Figure 2. Opacity, κ , opacity derivative, $\kappa_T + \kappa_{\rho}/(\Gamma_3 - 1)$, thermal timescale, τ_{th} (in days), and differential work integral, $dW/d\log T$ (arbitrary units, positive in driving zones), for selected pulsation modes ($\ell=1$), plotted versus temperature for representative models of β Cephei (left) and δ Scuti (right) variables. The dashed vertical lines mark the position of the maximum driving for the unstable modes shown in the lower panels. The horizontal lines in the τ_{th} diagrams correspond to the periods of selected modes.

overtone is stable because the damping above the metal bump region is activated due to their shorter periods (mode p_4 in Fig. 2). The longer period gravity modes are not excited both due to the timescale requirement in the metal bump region and due to stronger damping below this region.

In the model of a δ Scuti star, the mode p_1 (with a period of about 2 hours) is unstable due to the helium opacity bump which is connected with the second helium ionization zone. The mode p_8 is stable because due to its three times shorter period the damping between helium and hydrogen ionization zones is activated. Note that due to the very sharp hydrogen opacity bump there is also a small driving contribution from this region. The metal opacity bump is relatively small in this model. Moreover, the oscillation amplitudes are small in

deep layers. Therefore, the metal bump (and hence metal abundance) has only a weak influence on stability of the δ Scuti models. We confirm this conclusion later showing only a small sensitivity of the position of the δ Scuti instability domain to the choice of initial metal abundance.

3. Instability domain for a standard set of stellar parameters

3.1. Theoretical HR and the $\log g - \log T_{\text{eff}}$ diagrams.

In Fig. 3 we present the theoretical δ Scuti instability domain as computed with the latest version of the OPAL opacities (Iglesias & Rogers 1996). The models were computed without taking into account the effects of rotation and convective overshooting. An initial hydrogen abundance of $X = 0.70$ and a heavy element abundance of $Z = 0.02$ were assumed.

Near the ZAMS, the fundamental radial mode, p_1 , and seven consecutive overtones, p_2 to p_8 , can be excited. Note that the blue edge for the radial fundamental mode lies approximately in the center of the instability strip, far away from the general Blue Edge defined as the hotter envelope of unstable stellar models. The Blue Edges of the unstable regions are hotter for higher overtones. This can be easily understood if we consider the behaviour of the eigenfunctions (in particular, the fractional amplitude of the radial displacement) inside the star and also compare the period of a given mode with the thermal timescale in the main driving region. Near the Blue Edge of higher overtones, the fundamental mode and lower overtones are stable both due to larger amplitudes in the interior (which results in a relatively stronger damping just below the main driving region) and due to longer periods (which also results in a stronger influence of the deeper layers below the driving region if we use the thermal timescale argument for the instability occurrence, as it was discussed in Section 2).

For cooler stellar models at a fixed luminosity (or along an evolutionary track), the periods of oscillation are even longer. But the local thermal timescale in the second helium ionization zone is increasing even faster, which results in an decreasing influence of the underlying dissipative layers. Therefore, the lower overtones and the fundamental mode can be excited as well.

The modes p_9 and higher are stable because the damping region above second helium ionization zone is activated due to their short periods (the thermal timescale argument) and because of steeper gradients in their eigenfunctions, which result in smaller amplitudes in the potentially driving zone of second helium ionization.

Another important property of the blue edges is their curve for higher overtones. The symbol $p_6(\text{RE})$ in Fig. 3 marks a ‘‘Red Edge’’ for the mode p_6 produced due to a change in the slope of the Blue Edge for this mode in the same way as for the modes p_7 and p_8 . A similar effect of intersection of the fundamental and first overtone blue edges with the luminosity increase is well-known for the RR Lyrae star models. Cox, Castor & King (1972) explained such an intersection by the approach of a node in the radial displacement to the driving region, which causes a ‘‘quenching’’ of the first harmonic instability. The separation of the main driving region, the second helium ionization zone, from the node in radial displacement is determined primarily by the ratio M/R of the global stellar parameters. Our results confirm those of Stellingwerf (1979)

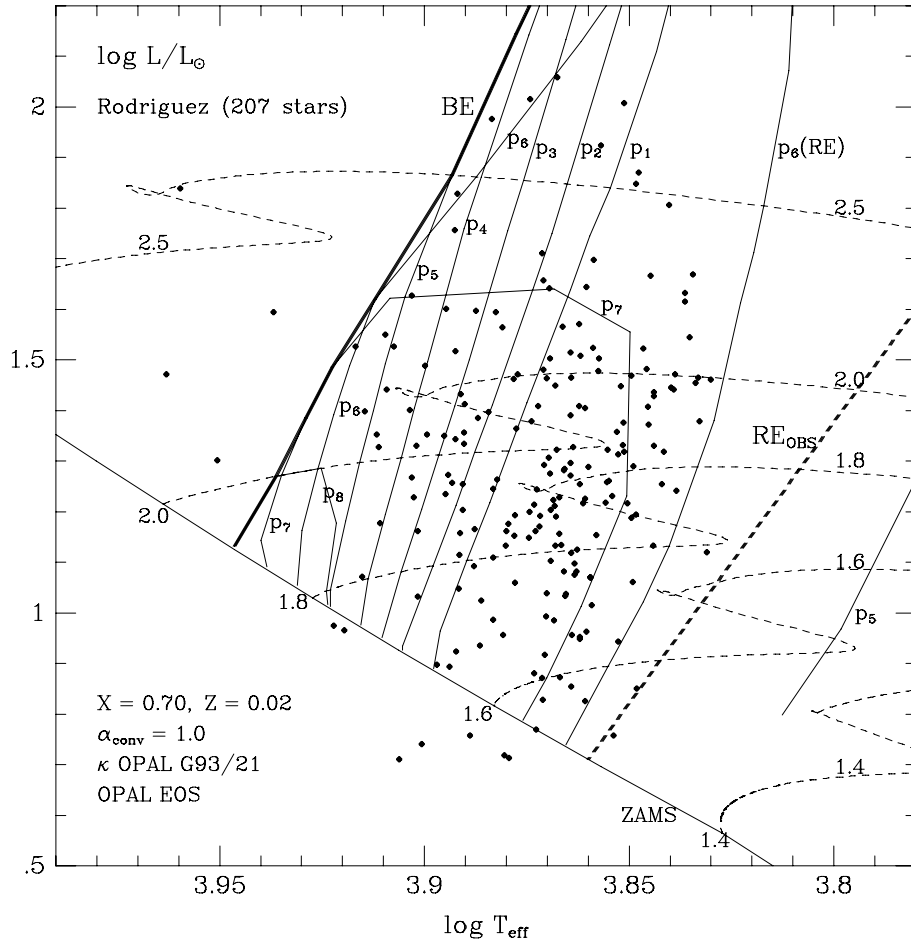


Figure 3. Theoretical Blue Edges of the δ Scuti instability domain for radial oscillations (symbols $p_1 - p_8$ mark corresponding modes, starting from fundamental one). The symbol BE stands for the general Blue Edge, which is the hotter envelope of unstable models. The symbol RE_{OBS} marks the empirical Red Edge. The Zero-Age Main Sequence (ZAMS) and a few evolutionary tracks for the indicated values of M/M_{\odot} are shown. Observational data are from the catalogue of Rodriguez et al. (1994). See text for details.

who concluded that the stabilization of the overtone pulsations (fourth and fifth in his study) is caused by the approach of the outermost node of the radial displacement to the driving region.

The Blue Edges computed in this way agree very well with our previous results based on earlier OPAL opacities (see Fig. 6 in Dziembowski, Moskalik & Pamyatnykh 1993, where the general Blue Edge of the δ Scuti instability domain is plotted together with instability domains of the SPB and β Cephei stars). There is also good agreement with our old results obtained with Los Alamos opacities for the fundamental radial mode and third overtone (Pamy-

atnykh 1975): old BE (p_1) lies close to BE (p_2), and Blue Edges for the third overtone, p_4 , are close to one another. This quite satisfactory agreement between results obtained with the OPAL and Los Alamos data are explained by the fact that in the most important region around the second helium ionization zone both series of opacities do not differ significantly; the main difference is confined to much deeper layers (the metal opacity bump at $T \sim 200\,000$ K is missing in the Los Alamos data) which have practically no effect on the δ Scuti-type instability near the Blue Edges.

Our blue edges BE(p1) and BE(p3) agree quite well with those by Stellingwerf (1979) (ours are slightly steeper). Note that Stellingwerf considered only stellar envelope models.

Blue edges of the δ Scuti domain computed by Li & Stix (1994) are significantly hotter. However, these results disagree with data about XX Pyxidis, whose lowest unstable mode frequency is that of mode p_4 or p_5 (see Pamyatnykh et al. 1998). To achieve agreement with the Li & Stix instability results, the star must be evolved and must have a mass of about $2.5 M_\odot$. However, calibrated photometric data give $\log g \approx 4.25$ which means that the star is located close to the ZAMS and its mass is about $1.9 M_\odot$.

To compare the position of the theoretical domain with the observations, we chose 207 stars with available $uvby\beta$ photometry from the catalogue of Rodriguez et al. (1994). Note that in the general HR diagram for the upper main-sequence stars (see Fig. 3 in Paper I, which is reproduced in Breger's review in these Proceedings) the observed 135 δ Scuti variables from the catalogue of Garcia et al. (1995) are plotted. The photometric data were transformed to effective temperature, T_{eff} , using the calibration due to Moon & Dworetzky (1985) (in practice, we used the program UVBYBETA written by Moon 1985 and modified by R. Napiwotzki). Stellar absolute magnitudes, M_V , were derived also with this program; the calculations are based on the relations of Strömgren (1966) and Crawford (1975, 1979), with some modifications. Finally, bolometric corrections to the absolute magnitudes were determined according to the calibration by Balona (1994).

Our comparison with the observations is rather illustrative. We do not discuss here the errors of calibrations, the positions of individual stars and we do not try to correct some data using additional information (like distances for the members of open clusters or according to the HIPPARCOS data). Our goal is to demonstrate the possibility of using different diagrams for such a comparison and to note some regularities.

As can be seen from Fig. 3, there is a quite good general agreement of the theoretical and observational domains of instability. Also, some regularities can be seen in this diagram. Approximately 25% of the variables are hotter than the Blue Edge for the radial fundamental mode, p_1 , so they must pulsate only in overtones. Also, many variables, approximately 30% of the total number, are located above the main sequence band, whose boundary is determined by the Terminal-Age Main Sequence (the TAMS line is not plotted in this figure; it connects the rightmost points of the MS part of each evolutionary track). The situation differs from that of β Cephei stars (see Paper I), nearly all of which are located on the main sequence. The explanation is very simple: the post-MS evolution of massive stars is very fast in comparison with the MS evolution,

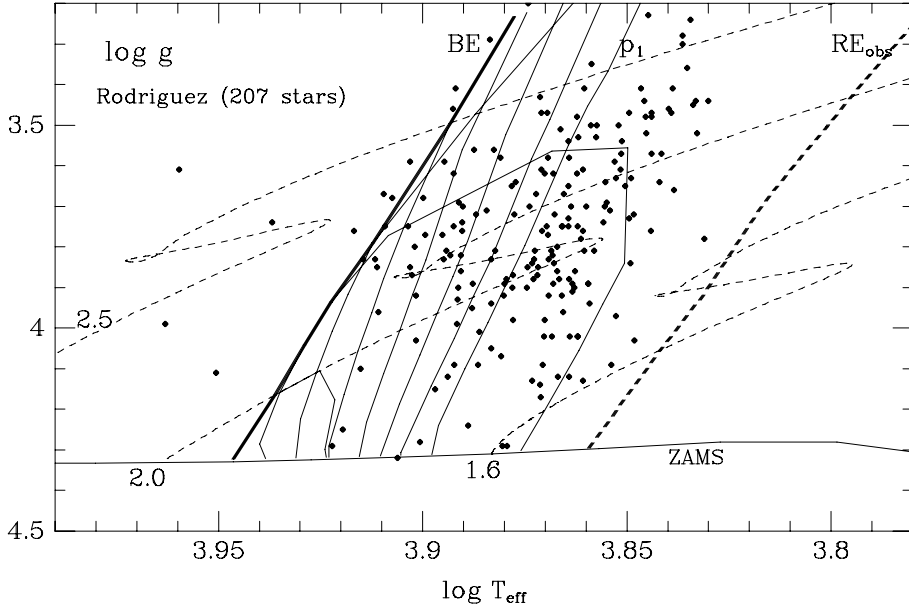


Figure 4. The δ Scuti instability domain in the $\log g - \log T_{\text{eff}}$ diagram. The same models and the same calibrations for observed stars as in Fig. 3 were used. A few evolutionary tracks for the indicated values of M/M_{\odot} are shown.

therefore we do not observe β Cephei variables during this stage. On the other hand, in the δ Scuti domain, the post-MS evolution is only 10 to 50 times faster than the MS evolution (see Breger & Pamyatnykh 1998). Moreover, selection effects (higher luminosities and statistically higher amplitudes of the post-MS variables) favour detecting the post-MS δ Scuti variables. Also, overshooting from the stellar convective core (see Sect. 4), if it exists, will result in a broadening of the main sequence band and thereby will influence the percentages of the MS and post-MS pulsators. In the future, we plan to study this problem in more detail.

A few stars are hotter than the general Blue Edge, as was noted by Rodriguez et al. (1994), who called for their systematic observations in order to compare with the theoretical predictions in detail (see also Schutt 1993). A standard photometric calibration may be wrong for these stars, if they are chemically peculiar. Also, the theoretical Blue Edge is hotter for higher helium abundance, as will be demonstrated in Section 5.

Moreover, a few stars are located under the ZAMS. Probably, they are chemically peculiar, as was discussed by Rodriguez et al. (1994). If this is the case, then a standard M_V calibration should not be applied to these stars.

In Fig. 4 the δ Scuti instability domain in the $\log g - \log T_{\text{eff}}$ diagram is shown. The same models as in Fig. 3 were used. The photometric data were transformed to T_{eff} and $\log g$, using the calibration due to Moon & Dworetzky (1985) (as for Fig. 3, we used the program UVBYBETA previously referred to).

If we compare the theoretical and observed instability domains, such a diagram seems to be more useful than the HR diagram because here we use only one calibration based on models of atmospheres. For the HR diagram (and for the $M_V - (b - y)_0$ diagram in Fig. 6 below), we used a separate calibration of the absolute magnitudes which is based on other data.

As for the HR diagram in Fig. 3, we see here a good agreement between theory and observations; most of the variables are located within the theoretical instability domain.

However, approximately 50% of the variables seem to be in a post-MS evolutionary stage in this diagram, in comparison with 30% for the HR diagram in Fig. 3. This difference may be caused by relatively fast rotation, which decreases the effective gravity due to centrifugal acceleration.

It is easy to estimate that in the region around the TAMS the centrifugal acceleration may reach about 20% of the gravity at $V_{\text{rot}} \approx 150$ km/sec and about 40% at $V_{\text{rot}} \approx 200$ km/sec, which results in a decrease in $\log g$ of 0.1 – 0.2. The shift of the star positions in Fig. 4 by 0.1 to higher $\log g$ values will result in a decrease of post-MS pulsators to approximately 30% of the total number, in agreement with our estimate for the HR diagram in Fig. 3. Moreover, the stars which are slightly hotter than the Blue Edge will be located within the theoretical instability domain after such a shift in gravity, also in agreement with the HR diagram in Fig. 3.

In Fig. 5 lines of constant period for the radial fundamental mode in the $\log g - \log T_{\text{eff}}$ diagram are shown. The same models as in Fig. 3 and 4 were used. Points mark the position of all evolutionary models of $1.5 - 2.5M_{\odot}$ used to obtain lines of constant periods by interpolation with the IDL graphics package. Using this plot and the calibrated $uvby\beta$ photometric data it is possible immediately to compare the observed period with the theoretical period of the radial fundamental mode for a model of normal chemical composition. Note that for the models of δ Scuti stars periods of the first, second and third radial overtones are approximately 77%, 62–64% and 52–54% of the fundamental period, respectively.

3.2. Instability domain in photometric coordinates

When comparing observational and theoretical data on instability domains, we can use an inverse approach in contrast to the transformation of the observed photometric indices to the theoretical parameters. Namely, we can try to transform the theoretical parameters, which determine the position of the models in the HR and $\log g - \log T_{\text{eff}}$ diagrams, to the observable photometric indices. To construct such diagrams, we used theoretical $uvby\beta$ indices which were computed by Lester, Gray & Kurucz (1986) using different Kurucz model atmospheres.

Note that the photometric calibrations of effective temperature and gravity of Moon & Dworetzky (1985) and of Lester et al. (1986) differ from one another. Fortunately, for relatively cool A and F stars with $T_{\text{eff}} \lesssim 8500$ K (practically all δ Scuti variables belong to this group) both calibrations give effective temperatures in good agreement with stellar temperature standards, as discussed by Napiwotzki et al. (1993a).

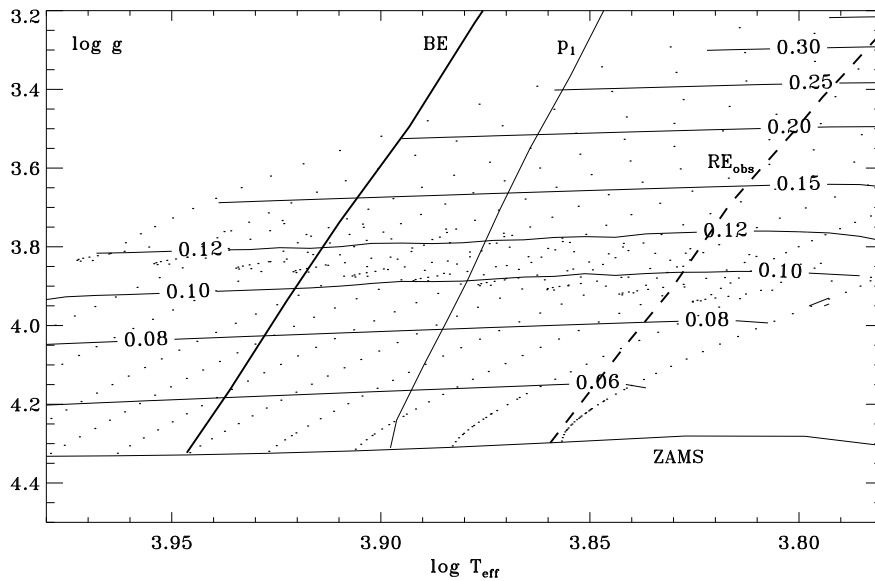


Figure 5. Lines of constant period for the radial fundamental mode in the $\log g - \log T_{\text{eff}}$ diagram. The same models as in Fig. 4 were used. Period values are given in days.

So, our diagrams in photometric coordinates will differ from previous theoretical diagrams not only in the coordinates themselves, but to some extent by using different calibrations.

Fig. 6 shows the δ Scuti instability domain in the $M_V - (b - y)_0$ diagram. The theoretical data from Fig. 3 (ZAMS line, evolutionary tracks and blue edges of the pulsational instability domain for different radial overtones) have been transformed to photometric indices according to the Lester, Gray & Kurucz (1986) tables for unpublished Kurucz grid for solar composition. Cubic spline interpolation in T_{eff} and $\log g$ has been used to obtain the theoretical $uvby\beta$ indices. The empirical Red Edge (RE_{obs}) according to Rodriguez et al. (1994) and Breger (1979) is also shown (note that the new empirical RE given by Breger in his review in these Proceedings is slightly steeper than the old one).

Different symbols have the same sense as in Fig. 3. The observational photometric data from the Rodriguez et al. (1994) catalogue have been dereddened according to the procedures of Crawford (1979) as they are implemented in the program UVBYBETA (Napiwotzki et al. 1993a).

Absolute magnitudes, M_V , were calculated also with this program using the relations of Strömberg (1966) and Crawford (1975, 1979) with some modifications.

For the stars with $T_{\text{eff}} \lesssim 8500$ K ($\log T_{\text{eff}} \lesssim 3.93$), the value of β , a measure of the equivalent width of the H_β line, is a good temperature indicator and c_0 , a measure of the strength of the Balmer discontinuity, is a good gravity parameter (see, for example, Napiwotzki et al. 1993a). Also, the color index $(b - y)_0$ is

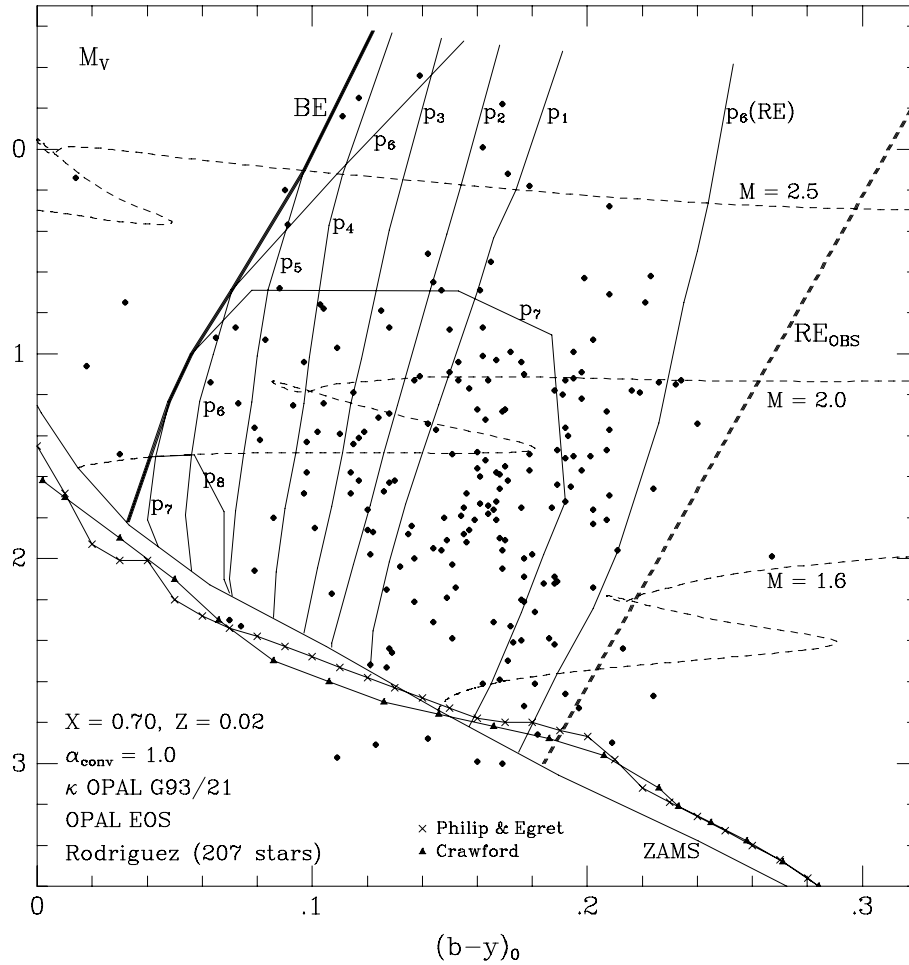


Figure 6. δ Scuti instability domain in the $M_V - (b - y)_0$ diagram. Empirical ZAMS lines (i.e., reference lines or unreddened standard relations between parameters) according to Crawford (1975, 1978, 1979) and Philip & Egret (1980) are marked by triangles and crosses, respectively.

a good temperature indicator. Practically all δ Scuti variables belong to this group of relatively cool stars.

We can see that there are systematic differences between the empirical and the theoretical ZAMS. The existence of this problem is demonstrated also by Breger for different calibrations in terms of stellar mass (see Fig. 7 of his review in these Proceedings). In addition to uncertainties in the photometric calibrations, we note that the position of the theoretical ZAMS is very sensitive to the choice of global stellar parameters, mainly to the initial chemical composition, as will be shown in Section 5.

There is a quite good agreement between theoretical and observational instability domains, with the same general regularities as in the theoretical HR diagram (Fig. 3).

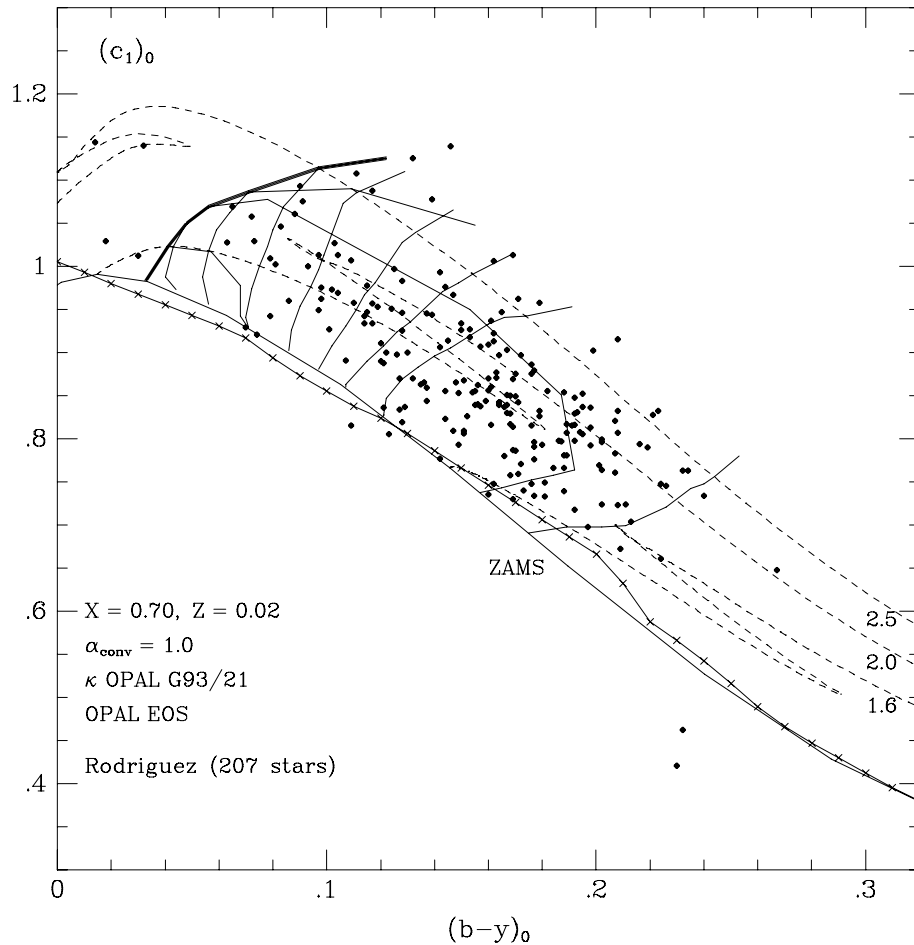


Figure 7. The δ Scuti instability domain together with the observational data from the Rodriguez et al. (1994) catalogue in the $(c_1)_0 - (b-y)_0$ diagram. The empirical reference line according to Philip & Egret (1980) is marked by crosses.

Figs. 7 and 8 show the δ Scuti instability domain in the $(c_1)_0 - (b-y)_0$ and in the $(c_1)_0 - \beta$ diagrams, respectively. As in Fig. 6, the theoretical data have been transformed to photometric indices according to the Lester, Gray & Kurucz (1986) tables for unpublished Kurucz grids for solar composition. The observational photometric data from the Rodriguez et al. (1994) catalogue have been dereddened using the UVBYBETA program.

Two stars below the ZAMS are the chemically peculiar variables AU Scl (Am-type) and XZ Men (δ Del-type). (Both in the $M_V - (b-y)_0$ diagram and in the theoretical diagrams of Figs. 3 and 4 they are located outside the parameter ranges of the figures). The luminosities of these stars are underestimated significantly (and gravities are overestimated) if we use a standard calibration of $uvby\beta$ photometry which is not valid for chemically peculiar stars (see discussion in Rodriguez et al. 1994).

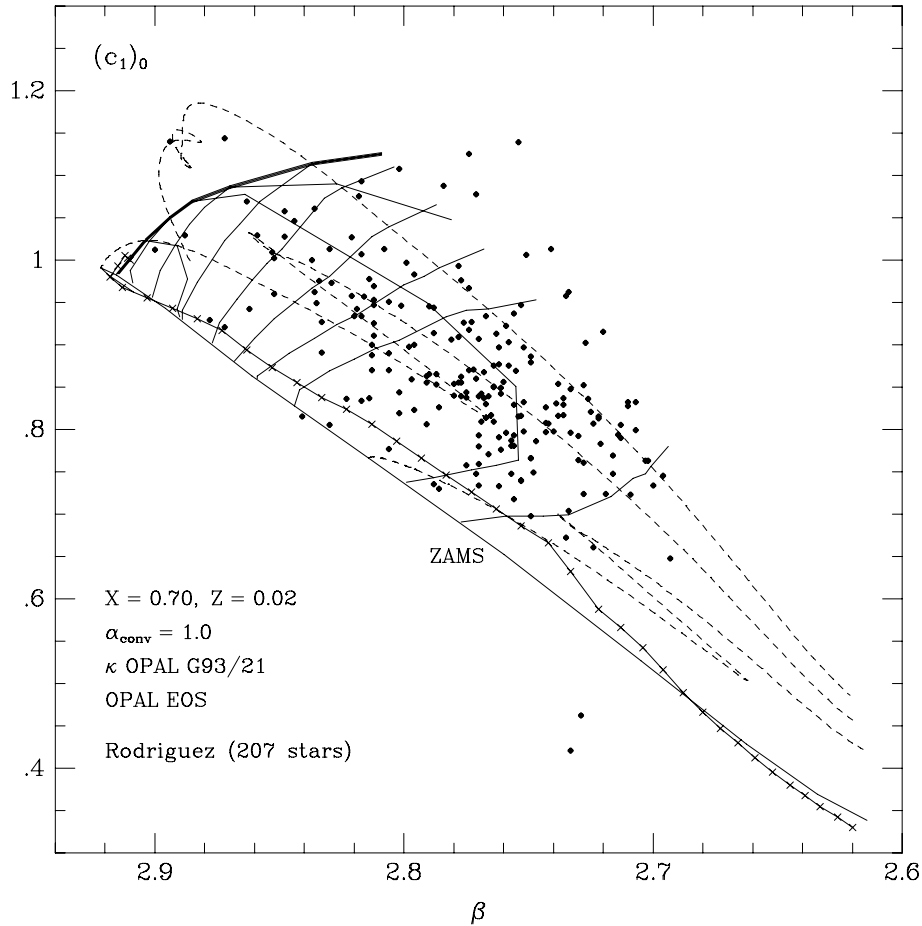


Figure 8. The δ Scuti instability domain together with the observational data from the Rodriguez et al. (1994) catalogue in the $(c_1)_0 - \beta$ diagram. The empirical reference line according to Philip & Egret (1980) is marked by crosses.

The systematic difference between the theoretical and the empirical ZAMS in Fig. 7 is qualitatively similar to that in Fig. 6. In our opinion, this similarity can be considered as an indication of the consistency of two separate photometric calibrations—the M_V calibration and the model atmosphere calibration used to obtain $\log g$ and $\log T_{\text{eff}}$ values. The last calibration was used to transform all theoretical lines from $\log g$, $\log T_{\text{eff}}$ coordinates to the photometric indices in Figs. 7 and 8. This difference between the theoretical and the empirical ZAMS is even more pronounced in Fig. 8. Here, we only demonstrate the effect which must be taken into consideration in detailed comparisons of observed data with theoretical models.

It can be seen from Fig. 8 that a lot of variables are located beyond the main sequence band (i.e., beyond the TAMS, which can be imaged as a line which connects the rightmost points of zigzag parts of different evolutionary tracks, much more than in the $M_V - (b - y)_0$ diagram (Fig. 6). A similar effect was

noted already in the $\log g - \log T_{\text{eff}}$ diagram as compared with the HR diagram (Figs. 4 and 3, respectively). It may be caused by stellar rotation which results in decreasing the effective gravity on the stellar surface and therefore changes the photometric index c_1 . Indeed, Crawford (1979) found a correlation between the δc_1 parameter (which is a measure of the distance from ZAMS) and the rotational velocity for the Pleiades and α Persei stars: the δc_1 index, which is sensitive to gravity, indicates a lower gravity for the more rapid rotators.

Crawford also noted that this effect may not be significant for most F stars which are rotating slower than A stars.

Lester et al. (1986) discussed the effect of rotation on the β index due to rotational broadening of the H_β line and due to the change of its equivalent width as a result of the rotational changes of the interior and the atmosphere structure. For a main-sequence model with $T_{\text{eff}} = 9500$ K the β index decreases by only 0.005 mag as the rotational velocity increases from 0 to 300 km/s.

Some stars in Fig. 8 are located to the right and to the top of most of the variables. From 6 stars here with known values of $v \sin i$, 4 stars have values between 140 and 190 km/sec.

4. Effects of convection, convective overshooting and stellar rotation

4.1. Effect of convection

To estimate the influence of the efficiency of convection in stellar envelopes on the position of the instability domain we computed a family of models completely neglecting convective energy transfer in the envelope (however, nothing was changed in the treatment of the convective stellar core) and studied their stability. The results of this test are presented in Fig. 9.

We can see that in the δ Scuti instability region convection in the envelope has no influence on the tracks and ZAMS position. A noticeable effect takes place only for the models with $M \lesssim 1.4M_\odot$.

Also, convection does not influence the position of the general Blue Edge. However, it changes the position of the radial fundamental Blue edge: $BE(p_1)$ is approximately 200 – 250 K cooler if convection is artificially suppressed in the stellar envelope. Such behavior is caused mainly by structural differences between convective and pure radiative models in the region of the hydrogen ionization which contributes to the driving of pulsations as well as in the main driving region of the second helium ionization. In our computations we neglect the Lagrangian variation of the convective energy flux during an oscillation cycle, i.e., we assume that the convective flux is at all times equal to the unperturbed value. This assumption is used generally (see, for example, Baker & Kippenhahn 1965). G.Houdek in these Proceedings discusses a more reliable theory for describing the interaction between convection and pulsation, taking into account dynamical effects of convection.

The convective energy flux is negligible in models near the general Blue Edge. But near the Blue Edge of the fundamental mode, convection can transfer up to 80–90 % of the energy in the center of the hydrogen ionization zone at temperatures of about 11000 K and therefore influence the structure of this zone. On the red edge, the convective contribution to the energy flux in the hydrogen

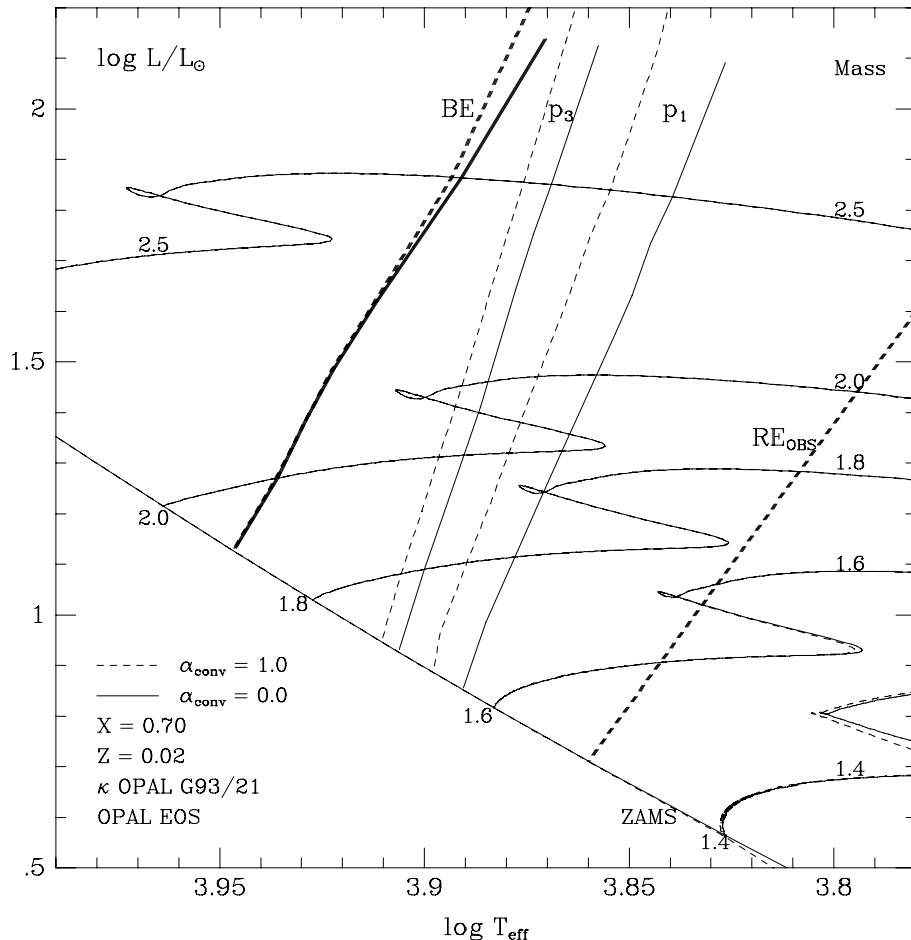


Figure 9. The effect of neglecting convection in the stellar envelope on the position of the blue edges of the δ Scuti instability domain. The Zero-Age Main Sequence (ZAMS) and a few evolutionary tracks for the indicated values of M/M_{\odot} are shown.

ionization zone may grow as large as 99%. Note that the efficiency of convection is negligible in the second helium ionization zone in all models within the δ Scuti instability domain. For example, in a $2 M_{\odot}$ model the convective contribution does not exceed 0.5% near the fundamental radial blue edge and 5% near the red edge.

4.2. The effect of overshooting from the stellar convective core

Some indications in favor of significant overshooting from the convective cores of δ Scuti stars were obtained from a comparison of evolutionary tracks with calibrated photometric data (e.g., Napiwotzki et al. 1993b). An asteroseismological test, based on the sensitivity of some nonradial mode frequencies to the size of the mixed stellar core, was proposed by Dziembowski & Pamyatnykh (1991).

To test the effects of overshooting explicitly, we computed a family of evolutionary tracks of $1.4\text{--}3.0 M_{\odot}$ for models with overshooting from the convective core and studied the stability of these models. The results are presented in Fig. 10. This figure is similar to that of Breger & Pamyatnykh (1998) where the Blue Edges are presented only for the standard models without overshooting.

The overshooting distance, d_{over} , was chosen to be $0.2 H_p$, where H_p is the local pressure scale height at the edge of the convective core. A similar value of the overshooting parameter was used by many authors (see, for example, Schaller et al. 1992, Napiwotzki et al. 1993b, Claret 1995).

The ZAMS models are identical in both cases (with and without overshooting) because they are chemically uniform.

The overshooting results in an extension of the MS-stage in the HR diagram due to an enlargement of the mixed core: more hydrogen fuel is available for nuclear burning. The displacement of the TAMS-points is about $\Delta(\log T_{\text{eff}}) = -0.02$, $\Delta(\log g) = -0.1$ to -0.15^2 . At a fixed effective temperature, a model with overshooting is slightly more luminous than a standard model without overshooting. Stellar lifetimes in the MS-stage are increased due to overshooting by 12–14%. At the TAMS, hydrogen is slightly more exhausted in models with overshooting: the central hydrogen abundance is about 4.0% (in mass) as compared with 4.5% in the case without overshooting.

It is interesting to compare stellar lifetimes in different evolutionary stages for the models with and without overshooting. Let us consider segments of the evolutionary tracks of the $1.8 M_{\odot}$ model in the effective temperature range between the TAMS and the leftmost point of the second contraction stage. The star crosses that region three times in its life on and beyond the MS. In the overshooting case ($\log T_{\text{eff}} = 3.8081 - 3.8671$, see Fig. 10) these times are equal to 0.35, 0.034, and 0.019 Gyr for MS, second contraction and post-MS expansion stages, correspondingly. In the standard case without overshooting ($\log T_{\text{eff}} = 3.8260 - 3.8769$) these times are equal to 0.35, 0.038, and 0.056 Gyr. We see that in both cases the second contraction times are similar and are one order of magnitude shorter than in the final part of the MS evolution. On the other hand, post-MS expansion in the overshooting case is a factor of 1.8 faster, and in the standard case a factor of 1.5 slower than the corresponding second contraction. Such a significant difference in the post-MS expansion times between evolution with and without overshooting seems to be important for statistical investigations of the distribution of the δ Scuti stars in the HR and similar diagrams.

Fig. 10 shows very clearly that overshooting from the convective core does not affect the position of the instability domain at all: the Blue Edges for the

² According to our computations with a given choice of d_{over} , overshooting influences the TAMS position 1.5–2 times less than according to Schaller et al. (1992), Napiwotzki et al. (1993) or Claret (1995). The disagreement may be caused by numerical effects as a test shows. To achieve a sufficient accuracy in the oscillation computations we need to rely upon more detailed stellar models than one uses usually in the evolutionary computations. For example, our typical $2.0 M_{\odot}$ MS model consists of approximately 1300 layers, and there are 135 models between the ZAMS and TAMS. If we increase both space and time step sizes by factor of about 7–8, i.e., use more crude space and time grids, we can reproduce the corresponding evolutionary track of Schaller et al. (1992) almost precisely.

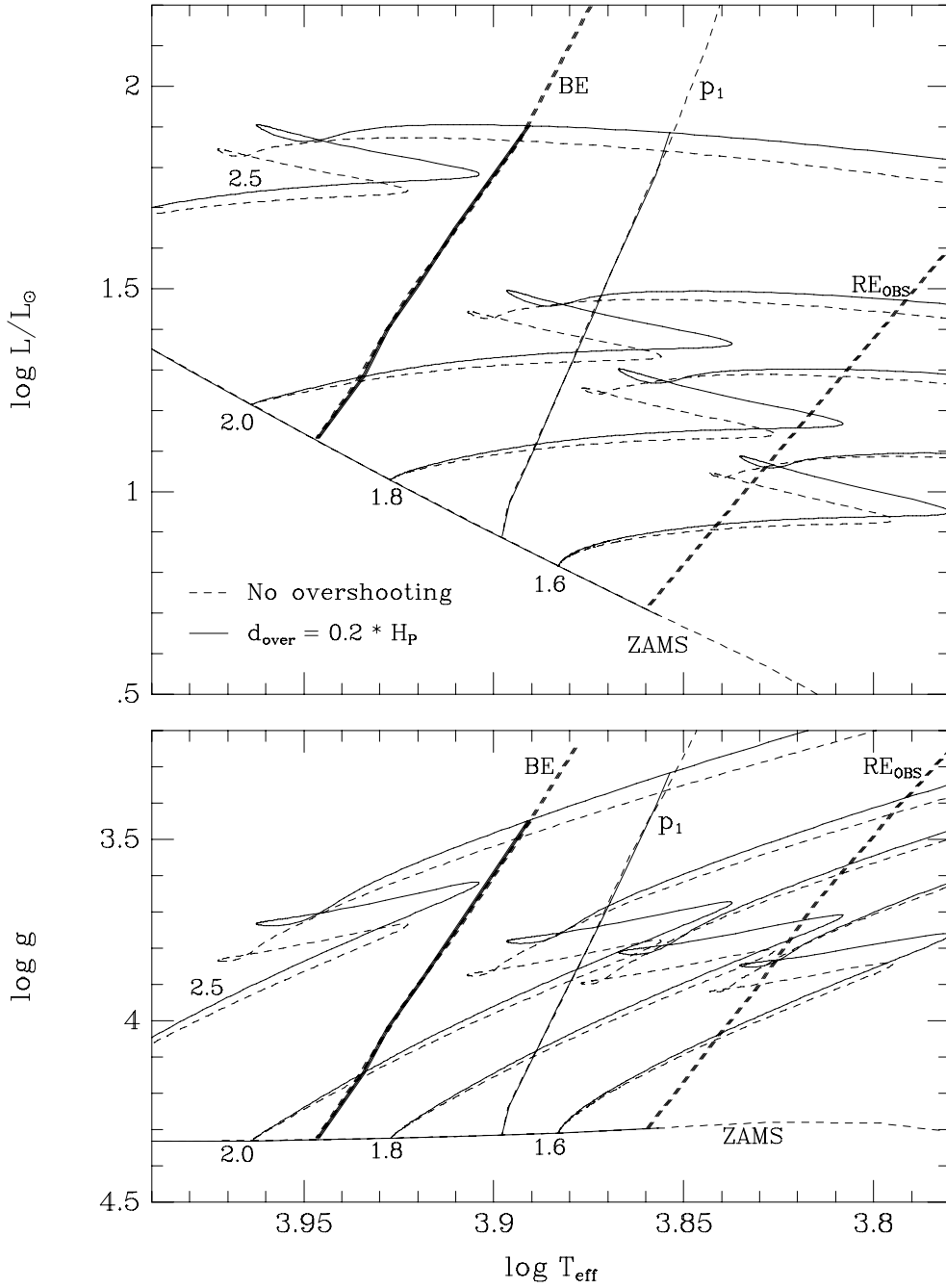


Figure 10. The effect of overshooting from the convective stellar core on the evolution and on the position of the blue edges of the δ Scuti instability domain in the HR and in the $\log g - \log T_{\text{eff}}$ diagrams. The Zero-Age Main Sequence (ZAMS) and a few evolutionary tracks for the indicated values of M/M_{\odot} are shown.

cases with and without overshooting coincide because the stellar envelope structure in both cases is very similar.

(In the same way, there must be no significant influence on the instability domain if we consider, for example, pre-MS stars which also differ mainly in their interior structure from MS stars. Parameters of the instability strip for pre-MS models have been computed by Marconi & Palla (1998). Our Blue Edge for the second overtone, p_3 , is hotter than that of Marconi & Palla by approximately 0.02 in $\log T_{\text{eff}}$. Such a difference needs to be explained in more detailed comparison of both computations which is beyond the scope of the present paper.)

Note that our studies of the β Cephei instability domain (Dziembowski & Pamyatnykh 1993, Pamyatnykh 1999) showed that for a normal chemical composition no overshooting is required to achieve a very good agreement between observed data and the period range of unstable radial modes in the main-sequence stellar models in the Period – $\log T_{\text{eff}}$ diagram. Also in the HR diagram no extension of the MS stage via convective overshooting is required to fit all β Cephei variables with the MS band quite well. We cannot test the overshooting theory in the same way for the δ Scuti stars because many variables are, probably, in the post-MS evolutionary stage and therefore a test based on the extent of the MS band cannot be applied in this case. As it was noted already (Dziembowski & Pamyatnykh 1991), there exists another asteroseismological test of convective overshooting theories but we do not yet have suitable observational data.

4.3. Effect of stellar rotation

An important parameter, which must influence stellar evolution and pulsations, is rotation. Detailed studies of non-evolutionary rotational effects on the oscillation frequency spectrum are beyond the scope of the present review; they are discussed by M.-J. Goupil et al. in these Proceedings. However, rotation significantly modifies the structure and evolution of a star.

In addition to the study by Goupil et al. we present here two more figures which illustrate the effect of rotation on stellar models and on the oscillation frequency spectrum. To this goal, we computed a family of evolutionary tracks of 1.4–3.0 M_{\odot} for rotating models.

We assumed uniform (solid-body) stellar rotation and conservation of global angular momentum during evolution from the ZAMS. These assumptions were chosen due to their simplicity. The same approach was used in our Paper I and in our papers on δ Scuti variables (see Breger et al. 1999 and references therein). The initial equatorial rotational velocity was assumed to be 150 km/s. The tracks for rotating and non-rotating models are shown in Fig. 11.

Rotation results in a shift of the tracks to smaller T_{eff} and gravity. The displacement of the TAMS mimics to some extent the overshooting effect, with $\Delta(\log T_{\text{eff}})$, $\Delta(\log g)$ smaller by a factor 1.5 in comparison with those for the overshooting case (compare Figs. 10 and 11). However, in contrast to the overshooting case, there is a noticeable shift of the ZAMS, especially in the $\log g - \log T_{\text{eff}}$ diagram. The tracks of rotating models lie slightly above the tracks of non-rotating models in the $\log g - \log T_{\text{eff}}$ diagram, and below the corresponding tracks in the $\log L - \log T_{\text{eff}}$ diagram which can be easily explained by a decreased effective gravity due to a horizontally averaged centrifugal force.

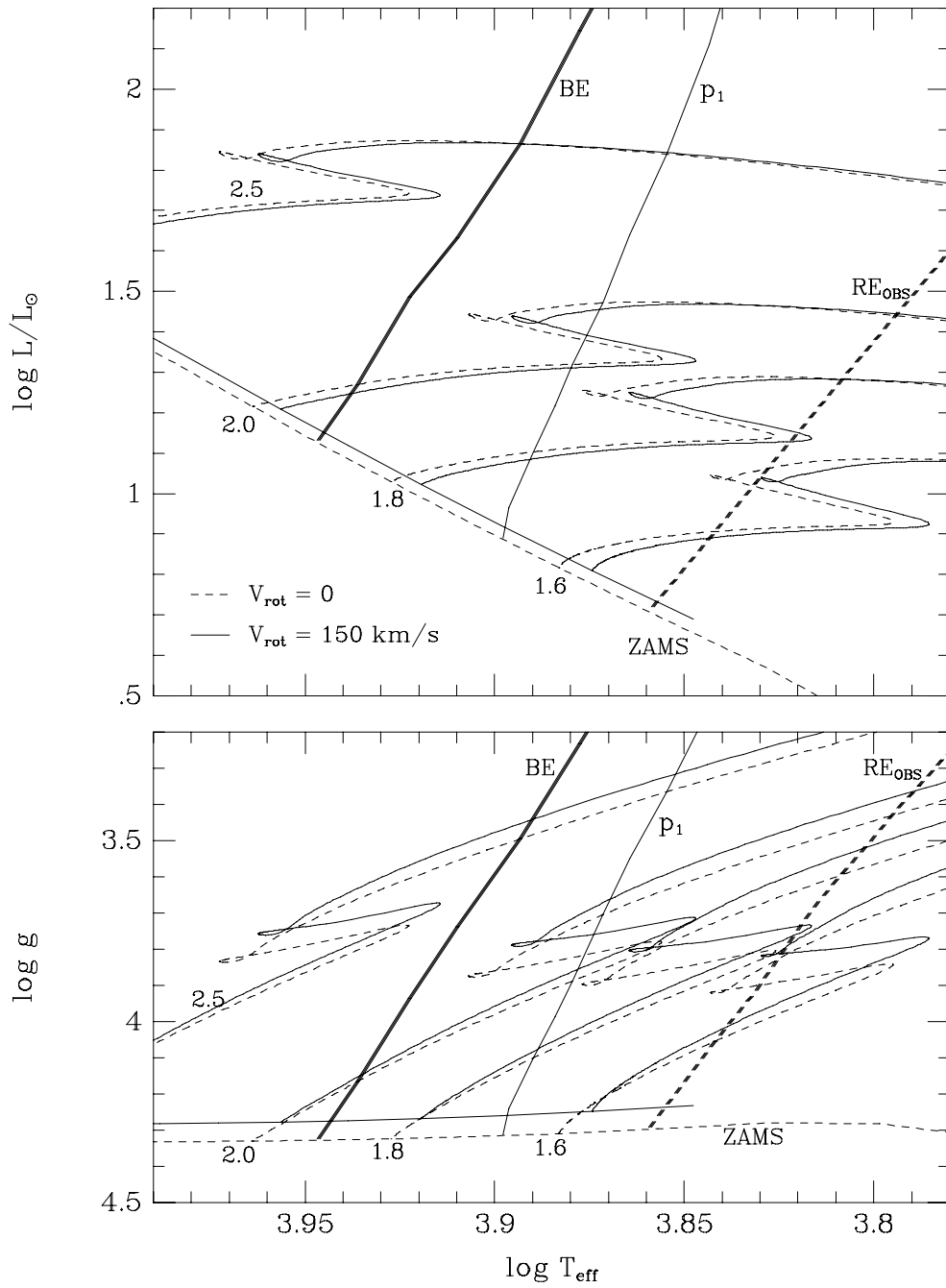


Figure 11. Evolutionary tracks of uniformly rotating (solid lines) and non-rotating (dashed lines) stellar models with masses 1.6, 1.8, 2.0 and 2.5 M_{\odot} . (See text for details.) The instability boundaries are the same as in Fig. 3.

The MS lifetime for rotating models is only 0.5–1.0% longer than that for non-rotating models. With our assumption of global angular momentum conservation, the equatorial rotational velocity decreases during the MS-evolution from 150 km/s on the ZAMS to about 120 km/s at the TAMS.

As has been noted by Goupil et al. in these Proceedings, differential rotation is likely to exist in main sequence stars and result in a mixing of chemical elements in the radiative interior. The evolutionary tracks for relevant stellar models are presented in the paper by Goupil et al. in these Proceedings. The mixing in the radiative stellar interiors influences the position of the track more strongly than a change of the stellar structure due to centrifugal acceleration. Therefore to obtain more realistic estimates of the rotation effects on the oscillation frequency spectrum and on instability we must take these effects into account.

However, here we present as an illustration the results assuming the simplest law of uniform rotation, in addition to the detailed discussion given by Goupil et al. in these Proceedings.

We did not compute yet the blue edges of the instability for rotating models, therefore only blue edges for the standard nonrotating models are given in the figure. According to computations by Lee & Baraffe (1995), the effects of centrifugal force and the resultant rotational deformation of the main-sequence stars do not affect significantly the pulsational instability of p - and g -modes.

The effects of slow rotation on the oscillation frequencies were treated up to third order in the rotational velocity (Dziembowski & Goode 1992, Soufi et al. 1998, Goupil et al. in these Proceedings).

Fig. 12 demonstrates the change in frequencies of low-degree modes in the observed frequency range of XX Pyxidis for models of different rotational velocities. The radial modes are the overtones p_4 , p_5 , p_6 .

The non-spherical deformation due to centrifugal force destroys the symmetry of the rotationally split multiplet; the effect is larger for higher p -mode frequencies. The asymmetry is already noticeable at a rotational velocity of about 40–50 km/sec. The effect of rotational coupling of nearly degenerate modes, which is not taken into account in the figure (see Goupil et al. in these Proceedings) results in additional perturbations to the frequency spectrum: close modes with degrees ℓ differing by an even integer and with the same m value are being repelled. This complicates the fitting of the observed and computed frequency spectra, as was demonstrated by Pamyatnykh et al. (1998) in an attempt to find a seismic solution to the 13 observed frequencies of XX Pyxidis.

It can also be seen that for $\ell = 2$ there are two close modes just before an avoided crossing. The mode with lower frequency is mainly a gravity mode, it has smaller asymmetry of the rotational splitting than the mode with higher frequency.

Finally, we note that in the nonlinear oscillation regime a coupling between modes within a multiplet may enforce an equidistant splitting, as it is discussed by Goupil et al. in these Proceedings.

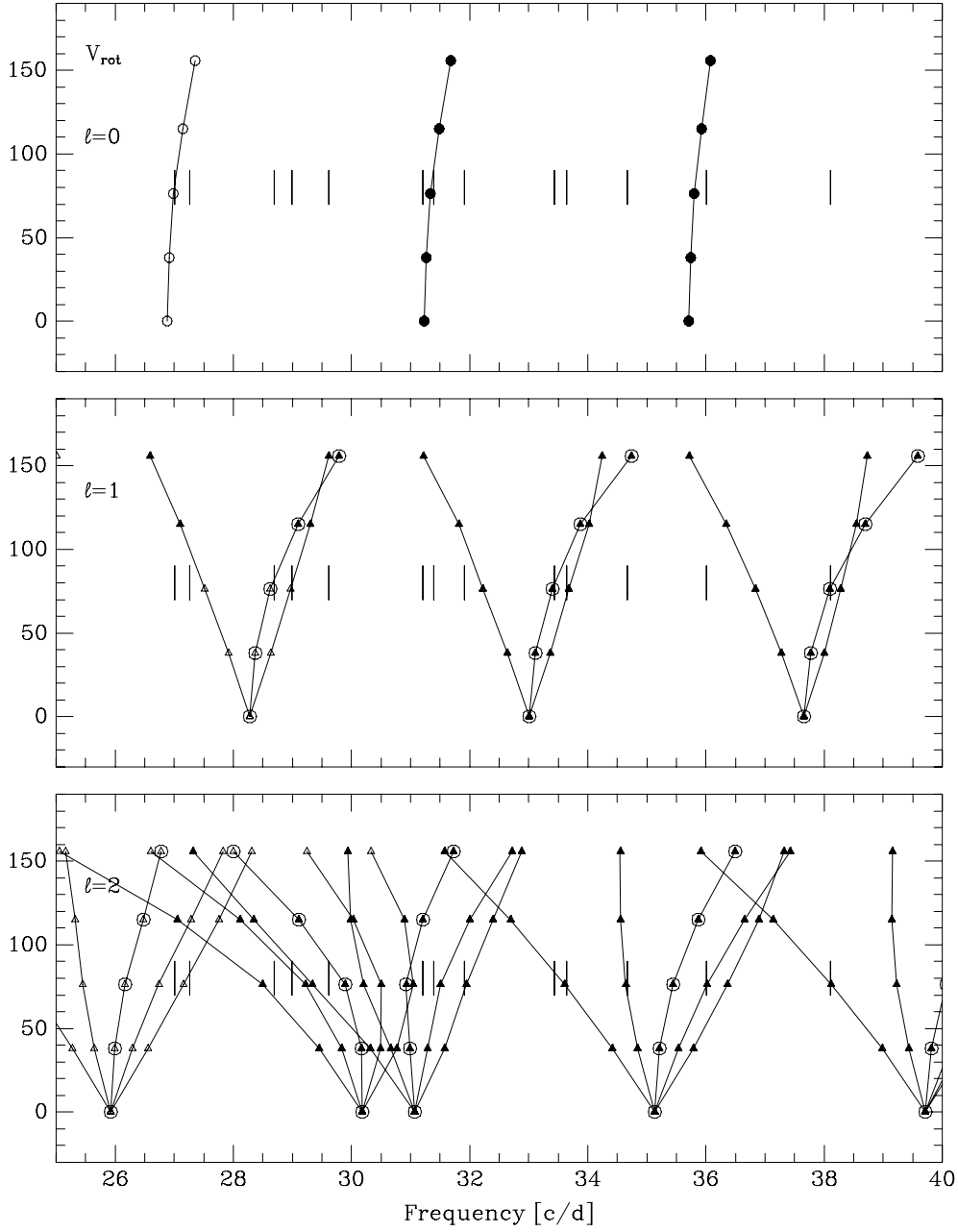


Figure 12. Rotational splitting of the frequencies of low-degree oscillation modes for models of $1.9 M_{\odot}$ near the Main Sequence. All models of different V_{rot} have the same effective temperature $\log T_{\text{eff}} = 3.91$. The luminosity of the models varies from $\log L = 1.21$ to $\log L = 1.23$ depending on V_{rot} (smaller for faster rotation). Vertical lines mark the observed frequency spectrum of XX Pyxidis.

5. Effects of variation of chemical composition

In Paper I we studied the sensitivity of the position of the β Cephei and SPB instability domains to variations in the initial abundance of hydrogen, X (or helium, Y), and heavy elements, Z . It was shown that the efficiency of the κ -mechanism acting in the region of the metal opacity bump is very sensitive to Z and much less sensitive to X , a result that is not surprising. For example, with decreasing Z the β Cephei instability domain shrinks down. At $Z = 0.01$ there are no unstable modes in the observed β Cephei region (cf. Fig. 3 in Paper I).

Here we show the results of similar tests for the δ Scuti instability domain. It was demonstrated in Section 2 that oscillations of the δ Scuti variables are excited mainly in the second helium ionization zone. Therefore, the efficiency of the κ -mechanism is not expected to be sensitive to the heavy element abundance but it should be strongly affected by the helium (or hydrogen) abundance.

5.1. Changing metallicity

In Fig. 13, we demonstrate the effect of variations in the heavy element abundance on the position of the blue edges of the δ Scuti instability domain. Indeed, the effect is insignificant. Smaller Z means a slightly higher helium abundance, Y , because we fixed the hydrogen abundance, X , at a standard value $X = 0.70$. Therefore, the driving in the second helium ionization zone is slightly more effective.

Note the very high sensitivity of the ZAMS line and evolutionary tracks to the heavy element abundance. The shift of a track of given mass to higher effective temperature and higher luminosity, when the Z value is decreasing, can be easily understood in terms of the opacity because a smaller Z value means a smaller value of the opacity in the interiors. Very simple and clear examples of the effect of opacity changes on evolutionary tracks were given almost twenty years ago by Fricke, Stobie & Strittmatter (1971). The width of the MS band decreases only slightly as Z decreases; the main effect of a Z decrease is a shift of the the MS as a whole.

We would like to stress that there exists a significant uncertainty in the stellar mass value for a given point in the HR or $\log g - \log T_{\text{eff}}$ diagrams due to uncertainties in chemical composition. Identified oscillation modes and good photometric calibrations may help to reveal some information about the chemical composition.

5.2. Changing initial hydrogen abundance

In Fig. 14 we show the effect of the hydrogen abundance change on the evolution and stability of the δ Scuti stars. Note, that in the $\log g - \log T_{\text{eff}}$ diagram, the ZAMS line practically does not change with X change. The ZAMS model of a fixed mass shifts along this line when the initial abundance has been changed. It can be seen also, that the decrease of the initial hydrogen abundance results in the narrowing of the MS band (less fuel is available for nuclear burning).

As expected, a change in X influences the position of the Blue Edges, but the effect appears to be very strong only for the general Blue Edge and for the blue edges of higher overtones; it becomes smaller for lower overtones and smallest for the radial fundamental mode. Approximately 25% of the shift of

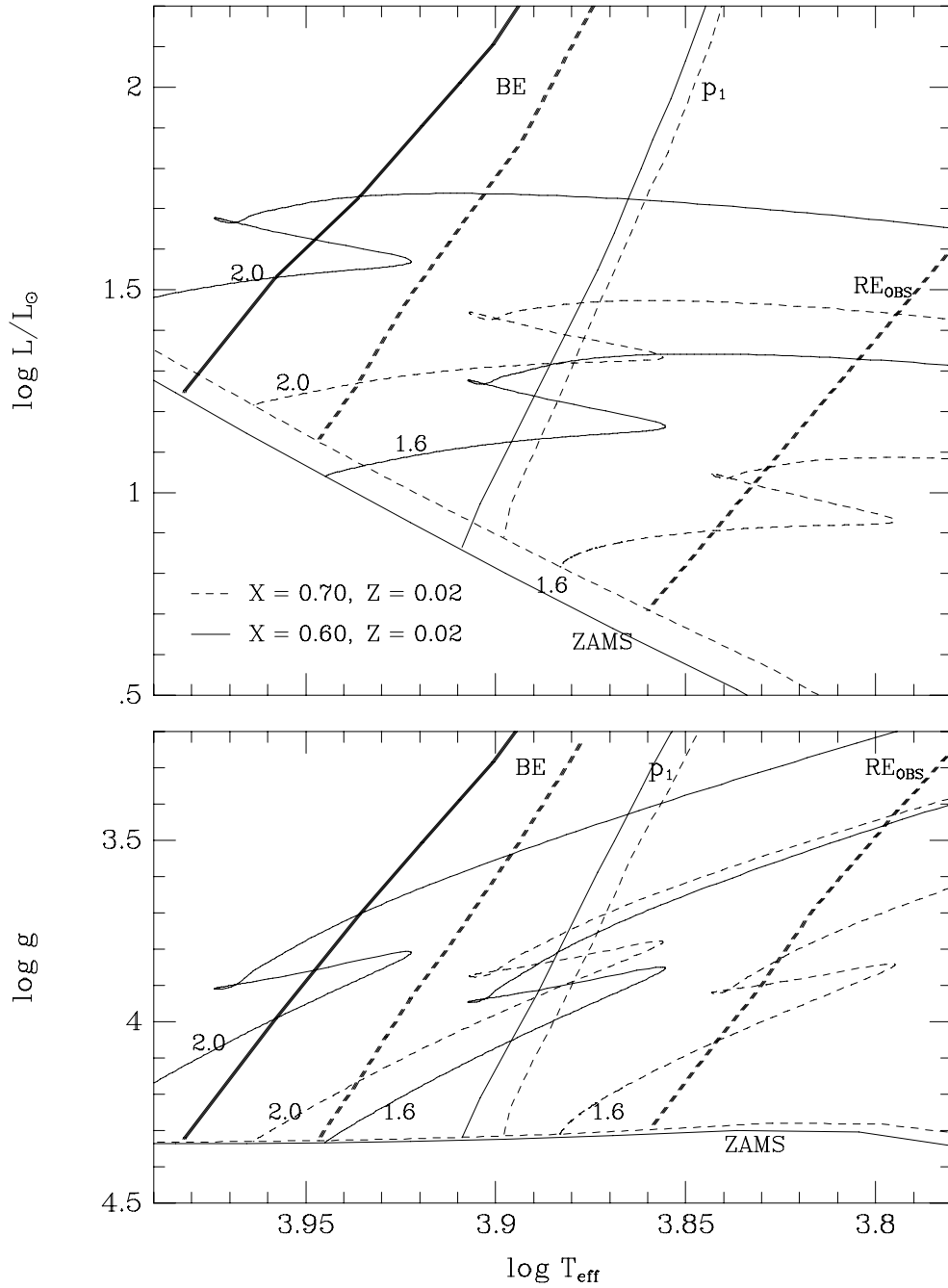


Figure 13. The effect of changes in the heavy element abundance on the evolution and stability of the models of δ Scuti stars. Dashed lines show the results obtained for the standard chemical composition $X = 0.70, Z = 0.02$ (Fig. 3 and 4). For both $Z = 0.01$ and 0.02 , the ZAMS lines and evolutionary tracks for the two indicated values of M/M_{\odot} are shown.

the general Blue Edge near the ZAMS to hotter effective temperatures is caused by the addition of the unstable overtone p_9 , which is not excited for the standard chemical composition.

The relatively small effect of a change in X on the fundamental Blue Edge position is caused by the fact that the increase of driving in the second helium ionization zone with increasing helium abundance is partly compensated by the decrease of driving in the hydrogen ionization zone which also contributes to the excitation of oscillations for the relatively cool stellar models near the fundamental radial Blue Edge. For hotter models near the general Blue Edge the hydrogen ionization zone does not contribute to the excitation of oscillations. We stress that the instability or stability of models near blue edges is determined by a quite small difference between strong driving and strong damping in relevant stellar layers.

The high sensitivity of the position of the general Blue Edge to the hydrogen (or helium) abundance can be used to estimate (constrain) these abundances in observed pulsating stars located close to the blue edges.

6. Discussion and some problems for future studies.

In this paper we presented the updated theoretical instability domain of the models of δ Scuti stars in various diagrams and studied the sensitivity of the position of the evolutionary tracks and the blue edges of the instability to changes in the global stellar parameters. In particular, we demonstrated that the convection theory parameters (mixing-length in the stellar envelope, the extent of the overshooting from the convective core) and the abundance of heavy elements do not influence the position of the general Blue Edge of the instability. In contrast, the high sensitivity of the position of the general Blue Edge to the hydrogen (or helium) abundance can be used to constrain these abundances in the observed pulsating stars located close to the blue edges.

We would like to summarize our results concerning the uncertainty of the ZAMS position due to initial chemical composition variations. Our computations show that at a fixed effective temperature of $\log T_{\text{eff}} \approx 3.9$, i.e., in the middle of the instability region on the ZAMS, the ZAMS line for $Z = 0.04$ lies above the ZAMS line for $Z = 0.01$ by $\Delta \log L \approx 0.28$, and the ZAMS line for $X = 0.80$ lies above the ZAMS line for $X = 0.60$ by $\Delta \log L \approx 0.16$. In the $\log g - \log T_{\text{eff}}$ diagram, the corresponding differences are $\Delta \log g \approx 0.135$ and $\Delta \log g \approx 0.015$, respectively. Note the practical insensitivity of the ZAMS to initial hydrogen abundance changes in the $\log g - \log T_{\text{eff}}$ diagram (Fig. 14); the effect is confined here to the displacement of a given stellar mass point along the ZAMS. The effect of the variations of the heavy metal abundances in the $\log g - \log T_{\text{eff}}$ diagram is seen very clearly. Such a difference in the ZAMS shift due to hydrogen and heavy element variations in the two diagrams can be potentially used to choose between changes of hydrogen or heavy element abundances when comparing observational data with the theoretical calculations.

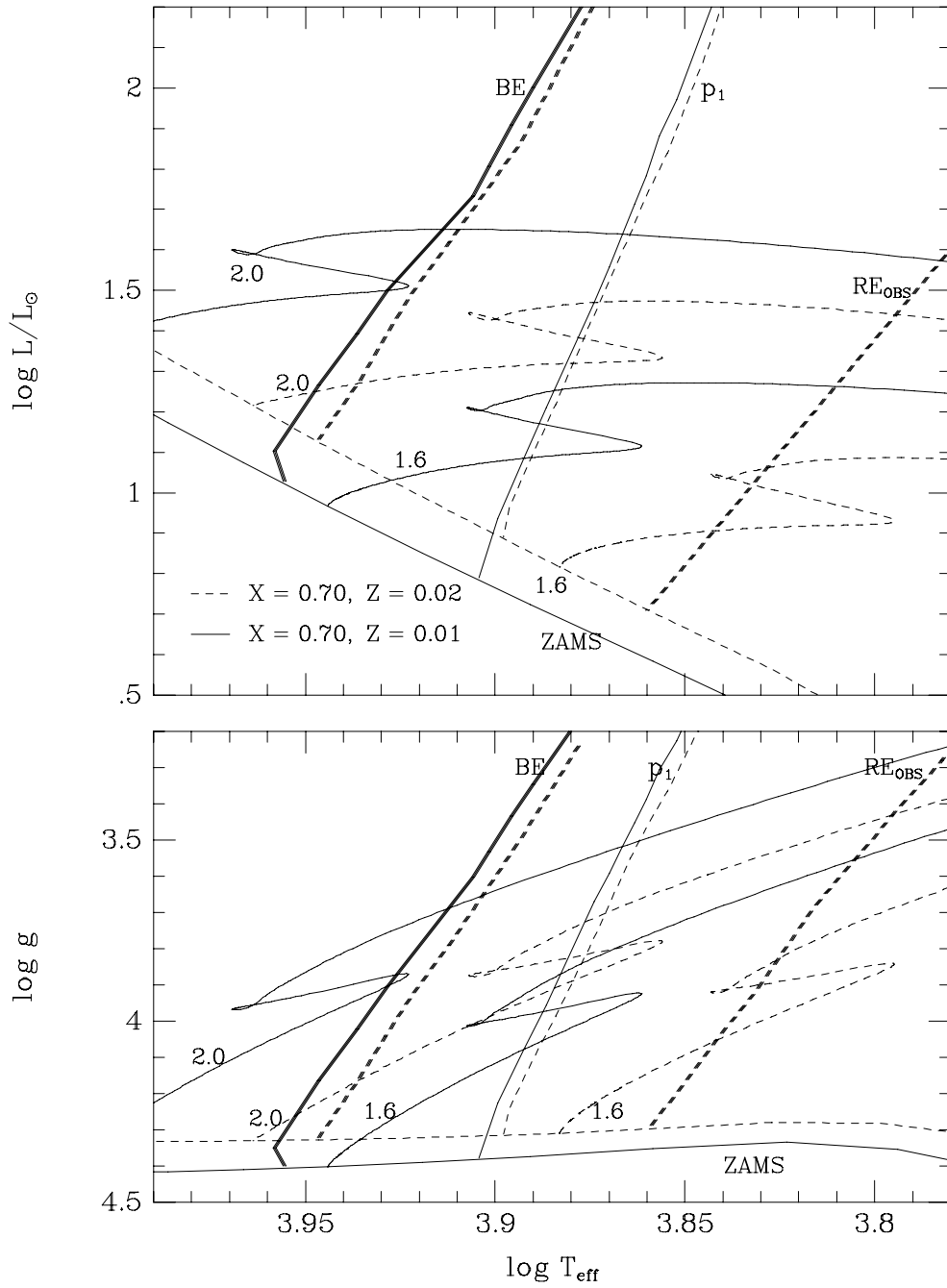


Figure 14. The effect of the hydrogen abundance change on the evolution and stability of the models of δ Scuti stars. Dashed lines show the results for the standard chemical composition $X = 0.70, Z = 0.02$ (Figs.3 and 4). For both $X = 0.60$ and 0.70 , the ZAMS lines and evolutionary tracks for the two indicated values of M/M_{\odot} are shown.

6.1. On the effect of using the OP opacities

All results presented in this paper were obtained using the OPAL opacities. To test the influence of the opacity choice on the instability, we computed a family of models using another set of opacities, namely, OP opacities (Seaton 1996).

The two series of opacity data differ from one another both due to completely independent approaches to calculate stellar opacities and due to small differences in heavy element abundances: the abundances of Ni differ by about 5%, and those of Ne, Cr and Fe by 2-3%. Note that all heavy element abundances are close to those for the solar mixture (Grevesse & Noels 1993). The computations with the OP opacities were performed using the same opacity interpolation routines as used for OPAL.

The OP opacities are systematically lower than OPAL in the deep stellar interiors. As was shown by Iglesias & Rogers (1995), these significant discrepancies are caused mainly by the fact that the OP atomic data neglect inner-shell photo-excitations which can contribute to the opacity. It was also shown by these authors that the OP approach makes approximations in the implementation of the occupation probability formalism that reduces the number of electrons in excited bound states. The combination of decreased excited level populations in OP plus the missing atomic data reduce the Rosseland mean opacity up to 30% at high densities and explain the observed discrepancies between OPAL and OP data.

Breger et al. (1999) computed models of a δ Scuti-type star, FG Virginis, both with OPAL and OP opacities. For these models, the difference in opacity is about 20% at temperatures above 10^6 K. In the envelope, at lower temperatures, the OP opacity varies slightly more monotonously along radius than does OPAL opacity: some dips are slightly shallower and some bumps are more flat. The differences do not exceed 8%: for example, at a temperature of 14 000 K the OP opacity is 4% smaller and at a temperature of 300 000 K it is 7.5% higher than the OPAL opacity.

The significant discrepancies in the very deep stellar interiors do not affect the instability which is caused by the second helium ionization zone at a temperature of about 50 000 K. We showed in Paper I that even the instability due to the metal opacity bump at a temperature of about 200 000 K, which is responsible for the β Cephei and SPB star oscillations, does not depend qualitatively on the choice between OPAL and OP opacities. In these driving regions the OPAL and OP data do not differ significantly.

Therefore, we do not expect any significant differences in the position of the Blue Edges of the δ Scuti instability domain when using OP instead of OPAL opacities. The explicit computations fully confirm this expectation; therefore, we do not present any diagram for the OP case.

Moreover, in the regions of helium and hydrogen ionization in stellar envelopes, the new OPAL and OP opacities do not differ significantly from the old Los Alamos opacities. Therefore our new results concerning the Blue Edges of the instability are in good agreement with earlier results obtained with Los Alamos data, as was noted in Section 3.

Note, however, that the smaller OP opacities in the deep interiors result in a shift of the evolutionary tracks to higher effective temperatures and luminosities, just like the shift of the tracks due a decrease in the metal abundance (Fig. 13).

6.2. Post-MS variables: 4 Canum Venaticorum as an example

To illustrate the complexity of the oscillation frequency spectra of evolved post-MS models of δ Scuti-type stars, we show in Fig. 15 the oscillation frequency spectrum for a model of 4 Canum Venaticorum which oscillates with at least 17 frequencies in the range 4.7–9.7 c/d. The ordinate gives the oscillatory moment of inertia (I) which is proportional to the oscillation kinetic energy and which is evaluated assuming the same radial displacement at the surface for each mode. The high density of the oscillation spectrum of nonradial modes is caused by very large values of the Brunt-Väisälä frequency in the deep interior.

The theoretical frequency range of unstable modes agrees very well with the observed range. Modes partially trapped in the envelope are characterized by a low value of I . The trapped modes are analogs of pure acoustic modes. It can be seen that the trapping is much more effective for dipole modes ($\ell = 1$) than for quadrupole modes ($\ell = 2$). The total number of unstable modes of $\ell \leq 2$ is equal to 449 taking into account the rotational splitting of each mode into $2\ell + 1$ components (only 111 unstable modes of azimuthal order $m = 0$ are shown in the figure).

So, if the model is correct, less than 4 percent of the unstable modes are excited to observable amplitudes. Potentially, the mode selection mechanism may be related to enhanced mode trapping in the envelope (Dziembowski & Królikowska 1990). It may be easier to excite them to a given amplitude on the surface. However, as it has been noted by Dziembowski (1997), “we do not know whether this effect has anything to do with mode selection. It is possible that the amplitudes are random quantities and that there is no rule of mode selection. Without such a rule we will never be able to make use of nonradial mode frequencies for seismic probing.”

In these Proceedings, Breger reports the observed spacing of about 1.2 c/d between identified $\ell = 1$ modes, but the theoretical spacing between trapped $\ell = 1$ modes in Fig. 15 is seen to be about 1.4 c/d. If we assume that we do observe the trapped modes then, to decrease the theoretical spacing, it is necessary to increase the stellar mass and/or to decrease the effective temperature in order to obtain $\log g \approx 3.3$, which is still within the allowed range based on the photometric calibrations.

6.3. On γ Doradus variables

Quite recently, a new group of variable F stars on the cool side of the δ Scuti instability domain was classified, γ Doradus variables (see a paper by A. B. Kaye in these Proceedings and also Kaye et al. 1999). Typical periods are from 0.4 to 3 days which corresponds to high-order gravity mode pulsations. The observational domain of these variables in the HR diagram is discussed by Handler (1999a). This instability region partly overlaps with that of the δ Scuti variables. As was noted by Handler (1999a) if stars exhibiting simultaneous γ Dor and δ Scuti-type pulsations could be found, this would increase the possibilities for asteroseismology of both classes of variables. Higher-frequency p -mode oscillations of δ Scuti-type can help constrain the mass and other global parameters of a star, and the high-order g -modes can be used to probe the deep interiors. One star with such a hybrid pattern of oscillations, HD 209295, was discovered very recently (Handler 1999b).

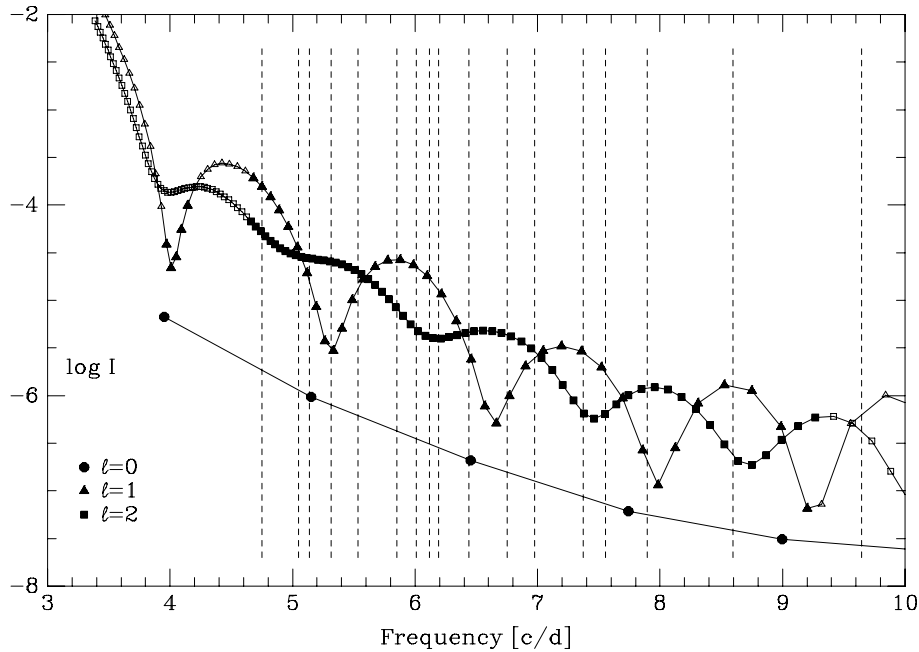


Figure 15. Oscillation frequencies in 4 Canum Venaticorum (shown as vertical lines) compared with those in an approximate model ($M = 2.3M_{\odot}$, $\log T_{\text{eff}} = 3.84$, $V_{\text{rot}} = 88$ km/sec, $\log g = 3.39$). The ordinate gives the oscillatory moment of inertia (I) which is evaluated assuming the same radial displacement at the surface for each mode. Only axesymmetric modes ($m = 0$) are shown. Open symbols denote stable modes. From Dziembowski (1997).

The theoretical δ Scuti instability domains in different diagrams can be used to make detailed comparisons with existing and future observed data on these stars.

Acknowledgments. The author thanks B. Paczyński, M. Kozłowski and R. Sienkiewicz for the stellar evolution code, M. Jerzykiewicz and R. Napiwotzki for the program UVBYBETA which transforms stellar photometric data into theoretical parameters, and M. Breger, J. Christensen-Dalsgaard, W. A. Dziembowski and M. H. Montgomery for helpful discussions and comments. This work has been supported in part by the grants RFBR-98-02-16734 and KBN-2-P03D-014-14. Part of the investigation has been supported by the Austrian Fonds zur Förderung der wissenschaftlichen Forschung, project number S7304.

References

- Aizenman, M. L., Smeyers, P., Weigert, A. 1977, *A&A*, 58, 41
 Alexander, D. R., Ferguson, J. W. 1994, *ApJ*, 437, 879
 Baglin, A., Breger, M., Chevalier, C., et al. 1973, *A&A*, 23, 221
 Bahcall, J. N., Pinsonneault, M. H. 1995, *Rev. Mod. Phys*, 67, 781

- Baker, N., Kippenhan, R. 1962, *Z. f. Astrophys.*, 54, 114
- Baker, N., Kippenhan, R. 1965, *ApJ*, 142, 868
- Balona, L. A. 1994, *MNRAS*, 268, 119
- Balona, L. A., Dziembowski, W. A. 1999, *MNRAS*, 309, 221
- Breger, M. 1979, *PASP*, 91, 5
- Breger, M., Pamyatnykh, A. A. 1998, *A&A*, 332, 958
- Breger, M., Pamyatnykh, A. A., Pikall, H., Garrido, R. 1999, *A&A*, 341, 151
- Claret, A. 1995, *A&AS*, 109, 441
- Chevalier, C. 1971, *A&A*, 14, 24
- Cox, J. P. 1963, *ApJ*, 138, 487
- Cox, J. P., Castor, J. I., King, D. S. 1972, *ApJ*, 172, 423
- Crawford, D. L. 1975, *AJ*, 80, 955
- Crawford, D. L. 1978, *AJ*, 83, 48
- Crawford, D. L. 1979, *AJ*, 84, 1858
- Dziembowski, W. A. 1977, *Acta Astron.*, 27, 95
- Dziembowski, W. A. 1995, in *GONG'94: helio- and astero-seismology*, eds. Ulrich R. K., Rhodes E. J., Jr., Däppen W., ASP Conf. Ser., vol. 76, p. 586
- Dziembowski, W. A. 1997, in *Sounding solar and stellar interiors*, Proc. IAU Symp. 181, eds. Provost J., Schmieider F.-X., Kluwer, Dordrecht, p. 317
- Dziembowski, W. A., Goode, P. R. 1992, *ApJ*, 394, 670
- Dziembowski, W. A., Królikowska, M. 1990, *Acta Astr.*, 40, 19
- Dziembowski, W. A., Moskalik, P., Pamyatnykh, A. A. 1993, *MNRAS*, 265, 588
- Dziembowski, W. A., Pamyatnykh, A. A. 1991, *A&A*, 248, L11
- Dziembowski, W. A., Pamyatnykh, A. A. 1993, *MNRAS*, 262, 204
- Fricke, K., Stobie, R. S., Strittmatter, P. A. 1971, *MNRAS*, 154, 23
- Garcia J. R., Cebal J. R., Scoccimarro E. R., Wahnnon, P., Arena, R., Bazterra, V., Pellizza, L., Risi, A., Rodriguez, M. L., Zimmermann, M. 1995, *A&AS*, 109, 201
- Grevesse, N., Noels, A. 1993, in *Origin and Evolution of the Elements*, eds. Pratz N., Vangioni-Flam E., Casse M., Cambridge Univ. Press., p. 15
- Handler, G. 1999a, *MNRAS*, 309, L19
- Handler, G. 1999b, *SAAO Newsletter No.33*,
- Iglesias, C. A., Rogers, F. J. 1995, *ApJ*, 443, 460
- Iglesias, C. A., Rogers, F. J. 1996, *ApJ*, 464, 943
- Kaye, A. B., Handler, G., Krisciunas, K., Poretti, E., Zerbi, F. M. 1999, *PASP*, 111, 840
- Lee, U., Baraffe, I. 1995, *A&A*, 301, 419
- Lester, J. B., Gray, R. O., Kurucz, R. L. 1986, *ApJS*, 61, 509
- Li, Y., Stix, M. 1994, *A&A*, 286, 815
- Marconi, M., Palla, F. 1998, *ApJ*, 507, L141
- Moon, T. T. 1985, *Comm. Univ. London Obs.*, No. 78

- Moon, T. T., Dworetzky, M. M. 1985, MNRAS, 217, 305
- Napiwotzki, R., Rieschick A., Blöcker T., Schönberner D., Wenske V. 1993b, in *Inside the stars*, Proc. IAU Coll. 137, eds. Weiss W. W., Baglin A., ASP Conf. Ser., vol. 40, p. 461
- Napiwotzki, R., Schönberner, D., Wenske, V. 1993a, A&A, 268, 653
- Pamyatnykh, A. A. 1975, in *Variable stars and stellar evolution*, Proc. IAU Symp. 67, eds. Sherwood V. E., Plaut L., Reidel, Dordrecht, p. 247
- Pamyatnykh, A. A. 1999, Acta Astron, 49, 119 (Paper I)
- Pamyatnykh, A. A., Dziembowski, W. A., Handler, G., Pikall, H. 1998, A&A, 333, 141
- Philip, A. G. D, Egret, D. 1980, A&AS, 40, 199
- Rodriguez, E., Lopez de Coca, P., Rolland, A., Garrido, R., Costa, V. 1994, A&AS, 106, 21
- Rogers, F. J., Swenson, F. J., Iglesias, C. A. 1996, ApJ, 456, 902
- Schaller, G., Schaerer, D., Meynet, G., Maeder, A. 1992, A&AS, 96, 269
- Schutt, R. L. 1993, PASP, 105, 22
- Seaton, M. J. 1993, MNRAS, 265, L25
- Seaton, M. J. 1996, MNRAS, 279, 95
- Soufi, F., Goupil, M.-J., Dziembowski, W. A. 1998, A&A, 334, 911
- Stellingwerf, R. F. 1979, ApJ, 227, 935
- Strömgren, B. 1966, ARA&A, 4, 433
- Zhevakin, S. A. 1963, ARA&A, 1, 367